

# Phase Transition from Mott Insulating Phase into the Charge Ordering Phase with Molecular Deformation in Charge-Transfer Salts $\kappa$ -(ET)<sub>4</sub>[M(CN)<sub>6</sub>][N(C<sub>2</sub>H<sub>5</sub>)<sub>4</sub>]·2H<sub>2</sub>O (M = Co<sup>III</sup> and Fe<sup>III</sup>)

Akira Ota,<sup>†,‡,§</sup> Lahcène Ouahab,<sup>\*,†</sup> Stéphane Golhen,<sup>†</sup> Yukihiro Yoshida,<sup>‡</sup> Mitsuhiro Maesato,<sup>‡</sup> Gunzi Saito,<sup>‡,||</sup> and Roman Świetlik<sup>⊥</sup>

*Organométalliques et Matériaux Moléculaires, Matériaux Inorganiques Multifonctionnels, UMR6226 CNRS, Université de Rennes 1, 263 Avenue Général Leclerc, CS74205, 35042 Rennes cedex, France, Division of Chemistry, Graduate School of Science, and Research Center for Low Temperature and Materials Sciences, Kyoto University, Sakyo-ku, Kyoto 606-8502, Japan Department of Chemistry, Graduate School of Science and Engineering, Tokyo Institute of Technology, 2-12-1-W4-1, O-okayama, Meguro-ku, Tokyo 152-8551, Japan, and Institute of Molecular Physics, Polish Academy of Sciences, Mariana Smoluchowskiego 17, 60-179 Poznan, Poland*

Received December 21, 2006. Revised Manuscript Received March 2, 2007

Two isostructural charge-transfer salts  $\kappa$ -(ET)<sub>4</sub>[M(CN)<sub>6</sub>][N(C<sub>2</sub>H<sub>5</sub>)<sub>4</sub>]·2H<sub>2</sub>O (ET = bis(ethylenedithio)-tetrathiafulvalene and M = Co<sup>III</sup>, Fe<sup>III</sup>) were synthesized, and their crystal structures, Raman spectra, electrical conductivities, electron spin resonance (ESR), and static magnetic susceptibilities as a function of temperature were studied. At room temperature the salts contain two crystallographically independent ET molecules with an average charge of +0.5. Temperature dependence of the Raman spectra revealed that a charge disproportionation gradually occurs upon cooling, because new peaks originated from the ET<sup>+</sup> and ET<sup>0</sup> grow gradually. ESR, static magnetic susceptibility, and conductivity data, supported by band structure calculation, give us firm evidence of the phase transition from the Mott insulating phase with the fluctuation of charge order into the long-range charge ordered phase at around 150 K. The charge ordered ground state consists of (ET<sup>+</sup>)<sub>2</sub> dimers and (ET<sup>0</sup>)<sub>2</sub> dimers, where the neutral molecules are found to be bent. The mechanism of this phase transition is discussed on the basis of crystallographic, spectroscopic, and magnetic features at various temperatures.

## 1. Introduction

Charge-transfer (CT) salts based on organic donors such as tetrathiafulvalene (TTF) or bis(ethylenedithio)-TTF (BEDT-TTF or ET) and their derivatives exhibit various electronic states and physical properties,<sup>1</sup> such as metallic conductivity or superconductivity,<sup>2</sup> Mott insulator or charge ordering (CO),<sup>3</sup> magnetic frustration,<sup>4</sup> and ferroelectricity.<sup>5</sup> One of the important features of CT salts is the narrow bandwidth (*W*), which is comparable to the on-site (*U*) and inter-site (*V*) Coulomb repulsion energies.<sup>3</sup> When *U* is larger than *W*, the system with a half-filled band becomes a Mott insulator as exemplified with  $\kappa$ -(ET)<sub>2</sub>Cu[N(CN)<sub>2</sub>]Cl.<sup>6</sup> In the case of a

quarter-filled band system, the strong inter-site Coulomb interaction (*V*) results in a CO state as observed in  $\theta$ -(ET)<sub>2</sub>MM'-(SCN)<sub>4</sub> (MM' = RbCo, RbZn, or CsZn) salts.<sup>7</sup> The CO phenomenon is much more interesting when it is coupled to lattice modulation accompanied with molecular deformations. For example, a drastic metal–insulator transition occurs in (EDO-TTF)<sub>2</sub>PF<sub>6</sub> (EDO-TTF = ethylenedioxy-TTF) salt associated with the deformation of the EDO-TTF molecule.<sup>8</sup>

\* To whom correspondence should be addressed. E-mail: ouahab@univ-rennes1.fr.

<sup>†</sup> Université de Rennes 1.

<sup>‡</sup> Division of Chemistry, Graduate School of Science, Kyoto University.

<sup>§</sup> Tokyo Institute of Technology.

<sup>||</sup> Research Center for Low Temperature and Materials Sciences, Kyoto University.

<sup>⊥</sup> Polish Academy of Sciences.

- (1) (a) *Chem. Rev.* **2004**, *104* (11), special issue. (b) *J. Phys. Soc. Jpn.* **2006**, *75* (5), special issue. (c) Ishiguro, T.; Yamaji, K.; Saito, G. *Organic Superconductors*, 2nd ed.; Springer-Verlag: Heidelberg, Germany, 1998. (d) Williams, J. M.; Ferraro, J. R.; Thorn, R. J.; Carlson, K. D.; Geiser, U.; Wang, H. H.; Kini, A. M.; Whangbo, M. H. *Organic Superconductors. Synthesis, Structure, Properties and Theory*; Prentice Hall, Englewood Cliffs, NJ, 1992.
- (2) (a) Ferraris, J. P.; Cowan, D. O.; Walatka, V., Jr.; Perlstein, J. H. *J. Am. Chem. Soc.* **1973**, *95*, 948. (b) Coleman, L. B.; Cohen, M. J.; Sandman, D. J.; Yamagishi, F. G.; Garito, A. F.; Heeger, A. J. *Solid State Commun.* **1973**, *12*, 1125. (c) Saito, G.; Enoki, T.; Toriumi, K.; Inokuchi, H. *Solid State Commun.* **1982**, *42*, 557. (d) Jerome, D.; Mazaud, A.; Ribault, M.; Bechgaard, K. *J. Phys. Lett.* **1980**, *41*, L95.

- (3) (a) Hiraki, K.; Kanoda, K. *Phys. Rev. Lett.* **1990**, *80*, 4737. (b) Seo, H.; Fukuyama, H. *J. Phys. Soc. Jpn.* **1997**, *66*, 1249. (c) Mazumdar, S.; Ramasesha, S.; Clay, R. T.; Campbell, D. K. *Phys. Rev. Lett.* **1999**, *82*, 1522. (d) Balicas, L.; Behnia, K.; Kang, W.; Canadell, E.; Aubab-Senzier, P.; Jerome, D.; Ribault, M.; Fabre, J. M. *J. Phys. I France* **1994**, *4*, 1539.
- (4) Shimizu, Y.; Miyagawa, K.; Kanoda, K.; Maesato, M.; Saito, G. *Phys. Rev. Lett.* **2003**, *91*, 107001.
- (5) (a) Tokura, Y.; Koshihara, S.; Iwasa, Y.; Okamoto, H.; Komatsu, T.; Koda, T.; Iwasawa, N.; Saito, G. *Phys. Rev. Lett.* **1989**, *63*, 2405. (b) Okamoto, H.; Mitani, T.; Tokura, Y.; Koshihara, S.; Komatsu, T.; Iwasa, Y.; Koda, T.; Saito, G. *Phys. Rev. B* **1991**, *43*, 8224. (c) Horiuchi, S.; Ishii, F.; Kumai, R.; Okimoto, Y.; Tachibana, H.; Nagaosa, N.; Tokura, Y. *Nat. Mater.* **2005**, *4*, 163.
- (6) (a) Kanoda, K. *Hyperfine Interact.* **1997**, *104*, 235. (b) Welp, U.; Fleshler, S.; Kwok, W. K.; Crabtree, G. W.; Carlson, K. D.; Wang, H. H.; Geiser, U.; Williams, J. M.; Hitsman, V. M. *Phys. Rev. Lett.* **1992**, *69*, 840.
- (7) (a) Mori, H.; Tanaka, S.; Mori, T.; Maruyama, Y. *Bull. Chem. Soc. Jpn.* **1995**, *68*, 1136. (b) Nakamura, T.; Minagawa, W.; Kinami, R.; Takahashi, T. *J. Phys. Soc. Jpn.* **2000**, *69*, 504. (c) Tajima, H.; Kyoden, S.; Mori, H.; Tanaka, S. *Phys. Rev. B* **2000**, *62*, 9378. (d) Yamamoto, K.; Yakushi, K.; Miyagawa, K.; Kanoda, K.; Kawamoto, A. *Phys. Rev. B* **2002**, *65*, 085110. (e) Seo, H. *J. Phys. Soc. Jpn.* **2000**, *69*, 805. (f) Clay, R. T.; Mazumdar, S.; Campbell, D. K. *J. Phys. Soc. Jpn.* **2002**, *71*, 1816.

In the so-called  $\kappa$ -phase salts the ET molecules within conducting layers are arranged in nearly perpendicular dimers, which interact with each other to yield a quasi-two-dimensional (Q2D) electronic structure. As a result of a strong dimerization in the  $\kappa$ -phase salts the electronic upper band can be considered as effectively half-filled, although it should be quarter-filled according to the stoichiometry.<sup>1,6</sup> In the  $\kappa$ -phase salts, the lowest Coulomb excitation is defined as an intra-dimer Coulomb energy ( $U_{\text{eff}}$ ) with two holes on each ET dimer. Because the parameter  $U_{\text{eff}}$  is comparable to  $W$ ,  $\kappa$ -salts can be classified as quasi-Mott-Hubbard.<sup>1,6</sup> Their transport properties are strongly dependent on subtle changes of temperature, pressure, and disorder, as well as the substitution of anions and chemical doping,<sup>9</sup> when they are located at the metal–insulator boundary.

The CO phenomena in the  $\kappa$ -phase salts with an effectively half-filled band are scarce, and only a few salts are reported, such as  $\kappa$ -(ET)<sub>4</sub>PtCl<sub>6</sub>·C<sub>6</sub>H<sub>5</sub>CN<sup>10</sup> and the triclinic  $\kappa$ -(ET)<sub>4</sub>[M(CN)<sub>6</sub>][N(C<sub>2</sub>H<sub>5</sub>)<sub>4</sub>]·3H<sub>2</sub>O (M = Co<sup>III</sup>, Fe<sup>III</sup>, and Cr<sup>III</sup>) salts.<sup>11</sup> However, details of their physical properties and their electronic states are not well-known. To understand the CO in the  $\kappa$ -phase salts and design new functional CT salts which would give rise to novel phase transitions, we synthesized new monoclinic salts, namely,  $\kappa$ -(ET)<sub>4</sub>[M(CN)<sub>6</sub>][N(C<sub>2</sub>H<sub>5</sub>)<sub>4</sub>]·2H<sub>2</sub>O (M = Co<sup>III</sup> (**1**) and Fe<sup>III</sup> (**2**)). We report here the phase transition from a Mott insulating phase with the fluctuation of charge order to a CO phase associated with molecular deformations and discuss the roles of electron correlations ( $U$  and  $V$ ), lattice-coupled effects due to the flexibility of molecule, electrostatic interactions between donor and anion layers, and spin degree of freedom in the transition.

## 2. Experimental Section

Single crystals of the isostructural title salts were obtained by electrochemical oxidation of ET in the presence of the electrolyte, [N(C<sub>2</sub>H<sub>5</sub>)<sub>4</sub>]<sub>3</sub>[M(CN)<sub>6</sub>] (M = Co<sup>III</sup> or Fe<sup>III</sup>). The crystals were grown on a Pt electrode (1 mm in diameter) in a U-shape cell separated by a sintered-glass filter in a mixture of acetonitrile and dichloromethane (1:4). The single crystals were mounted on a four circle diffractometer (CDFIX center of Université de Rennes 1) equipped with a CCD camera and a graphite monochromated Mo K $\alpha$

radiation source ( $\lambda = 0.71073 \text{ \AA}$ ). Data collection was performed at room temperature (RT) and 200 K for both compounds, and at 100 K for **1** and 106 K for **2**. The crystal structures were solved with SHELXS-97 and refined with SHELXL-97 programs by full matrix least-squares method on  $F^2$  of the unique data.<sup>12</sup> Crystal data for (**1**): monoclinic,  $P2_1/n$ ,  $Z = 2$  with the following parameters at  $T = 293, 200, 100 \text{ K}$ ;  $a = 11.276(2), 11.2307(3), 10.9798(5) \text{ \AA}$ ,  $b = 8.917(1), 8.8363(2), 8.8047(4) \text{ \AA}$ ,  $c = 38.176(6), 37.964(1), 38.579(2) \text{ \AA}$ ,  $\beta = 91.960(1), 91.934(1), 90.153(2)^\circ$ ,  $V = 3836(3), 3765.3(2), 3729.6(4) \text{ \AA}^3$ ,  $R_1(I > 2\sigma(I)) = 0.0511, 0.0614, 0.0727$ . Crystal data for (**2**): monoclinic,  $P2_1/n$ ,  $Z = 2$  with the following parameters at  $T = 293, 200, 106 \text{ K}$ ;  $a = 11.261(2), 11.2203(3), 11.0498(6) \text{ \AA}$ ,  $b = 8.941(5), 8.8587(3), 8.8371(6) \text{ \AA}$ ,  $c = 38.433(5), 38.054(1), 38.573(3) \text{ \AA}$ ,  $\beta = 91.463(5), 91.860(9), 90.142(1)^\circ$ ,  $V = 3868(3), 3780.5(2), 3766.6(4) \text{ \AA}^3$ ,  $R_1(I > 2\sigma(I)) = 0.0403, 0.0412, 0.0778$ . The complete crystal structure data are given in the CIF file in Supporting Information. Different single crystals of the same phase were measured at each temperature. Because of the fragility and relatively small size of the crystals, it was impossible to set properly the carbon atoms of the (C<sub>2</sub>H<sub>5</sub>)<sub>4</sub>N<sup>+</sup> cation at low temperature. The carbon atoms were isotropically refined for **2** at 106 K, whereas their coordinates and anisotropic thermal factors were fixed for **1** at 100 K.

The Fourier transform near-infrared (FT-NIR) Raman spectra were obtained using a Bruker Fourier IFS 66 spectrometer with a FRA 106 Raman attachment, which operates with a Nd:YAG laser with a wavelength of 1064 nm. It is well-known for organic conductors that a strong electronic absorption yields the problem of sample overheating, and therefore, the crystals were ground into a powder with KBr. This powdered form allowed us to investigate the spectra with a laser power of about 20 mW without sample deterioration. Each spectrum was accumulated over about 100 min (3000 scans). The scattered light was collected in a backscattering geometry; the spectral resolution was 4 cm<sup>-1</sup>. Low temperature measurements, down to 90 K, were performed with the samples mounted in a continuous-flow liquid-nitrogen Linkam THMS 600 cryostat (without the evacuation of the water molecules in the crystals). The cooling rate was less than 1 K min<sup>-1</sup>. The X-band ESR spectra were recorded with a JEOL JES TE-200 X-band spectrometer equipped with a TE<sub>011</sub> cavity and Oxford ESR910 cryostat in the temperature range of 4–300 K with an applied cooling rate approximately equal to 50 K h<sup>-1</sup>. The absolute value of the spin susceptibility ( $\chi_{\text{spin}}$ ) was determined with reference to the signal of CuSO<sub>4</sub>·5H<sub>2</sub>O, whose  $\chi_{\text{spin}}$  value is known to be 6.00 × 10<sup>-6</sup> emu g<sup>-1</sup> at 290 K. The sample crystal was mounted on a flat face cut on a quartz rod, using silicone grease. The measurements were performed under helium gas flow, not in the vacuum, to avoid the removal of the water molecules from the crystals.

The static magnetic susceptibility ( $\chi$ ) measurements were performed on microcrystalline samples with a Quantum Design MPMS-XL SQUID magnetometer with an applied field of 1 T between 1.9 and 350 K. Because the crystals lose the water molecules in the vacuum as mentioned above, the sample was sealed in a quartz tube under a helium atmosphere. The electrical resistivity measurement of **2** was performed within the crystal plane, using the four-probe direct current method by attaching gold wires (15  $\mu\text{m}$  in diameter) on a plate-like crystal (0.5 × 0.1 × 0.1 mm<sup>3</sup>) with carbon paste. Although the crystals of **1** were not large enough for the accurate resistivity measurements, it showed similar results

- (8) (a) Ota, A.; Yamochi, H.; Saito, G. *J. Mater. Chem.* **2002**, 2600. (b) Chollet, M.; Guerin, L.; Uchida, N.; Fukaya, S.; Shimoda, H.; Ishikawa, T.; Matsuda, K.; Hasegawa, T.; Ota, A.; Yamochi, H.; Saito, G.; Tazaki, R.; Adachi, S.; Koshihara, S. *Science* **2005**, 307, 86.  
 (9) (a) Komatsu, T.; Matsukawa, N.; Inoue, T.; Saito, G. *J. Phys. Soc. Jpn.* **1996**, 65, 1340. (b) Drozdova, O. O.; Saito, G.; Yamochi, H.; Ookubo, K.; Yakushi, K.; Uruichi, M.; Ouahab, L. *Inorg. Chem.* **2001**, 40, 3265. (c) Saito, G.; Ookubo, K.; Drozdova, O. O.; Yakushi, K. *Mol. Cryst. Liq. Cryst.* **2002**, 380, 23. (d) Ito, H.; Ishiguro, T.; Kubota, M.; Saito, G. *J. Phys. Soc. Jpn.* **1996**, 65, 2987.  
 (10) (a) Galimzyanov, A. A.; Ignat'ev, A. A.; Kushch, N. D.; Laukhin, V. N.; Makova, M. K.; Merzhanov, V. A.; Rozenberg, L. P.; Shibaeva, R. P.; Yagubskii, E. B. *Synth. Met.* **1989**, 33, 81. (b) Doublet, M. L.; Canadell, E.; Shibaeva, R. P. *J. Phys. I France* **1994**, 4, 1479.  
 (11) (a) Le Maguerès, P.; Ouahab, L.; Conan, N.; Gomez-García, C. J.; Delhaès, P.; Even, J.; Bertault, M. *Solid State Commun.* **1996**, 97, 27. (b) Le Maguerès, P.; Ouahab, L.; Briard, P.; Even, J.; Bertault, M.; Toupet, L.; Ramos, J.; Gomez-García, C. J.; Delhaès, P. *Mol. Cryst. Liq. Cryst.* **1997**, 305, 479. (c) Le Maguerès, P. Ph.D. Thesis, University of Rennes 1, Rennes, 1997. (d) Ouahab, L.; Golhen, S.; Le Hoerff, T.; Guillevic, J.; Tual, L.; Hérou, N.; Amiel, J.; Delhaès, P.; Binet, L.; Fabre, J. M. *Synth. Met.* **1999**, 102, 1642. (e) Swietlik, R.; Połomska, M.; Ouahab, L.; Guillevic, J. *J. Mater. Chem.* **2001**, 11, 1313.

- (12) (a) Otwinowski Z.; Minor, W. In *Processing of X-ray Diffraction Data Collected in Oscillation Mode*; Methods in Enzymology, Volume 276: Macromolecular Crystallography, part A; Carter, C. W., Jr., Sweet, R. M., Eds.; Academic Press: New York, 1997; pp 307–326. (b) Sheldrick, G. M. *SHELX 97, Program for the Refinement of Crystal Structures*; University of Göttingen, Göttingen, Germany, 1997.

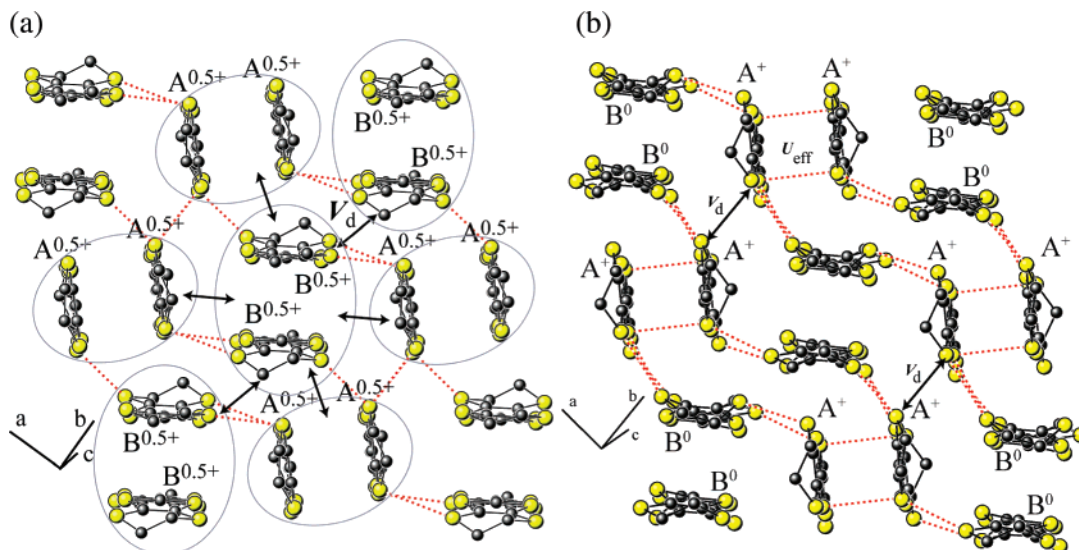


**Figure 1.** Donor layer of **1** viewed along the molecular long axis of ET (a) at RT and (b) at 100 K. Dashed lines indicate the S...S contacts shorter than the sum of van der Waals radii (3.60 Å). An oval corresponds to a hole delocalized on the  $(\text{ET}^{0.5+})_2$  dimer ( $U_{\text{eff}}$  and  $V_d$  are explained in the text).

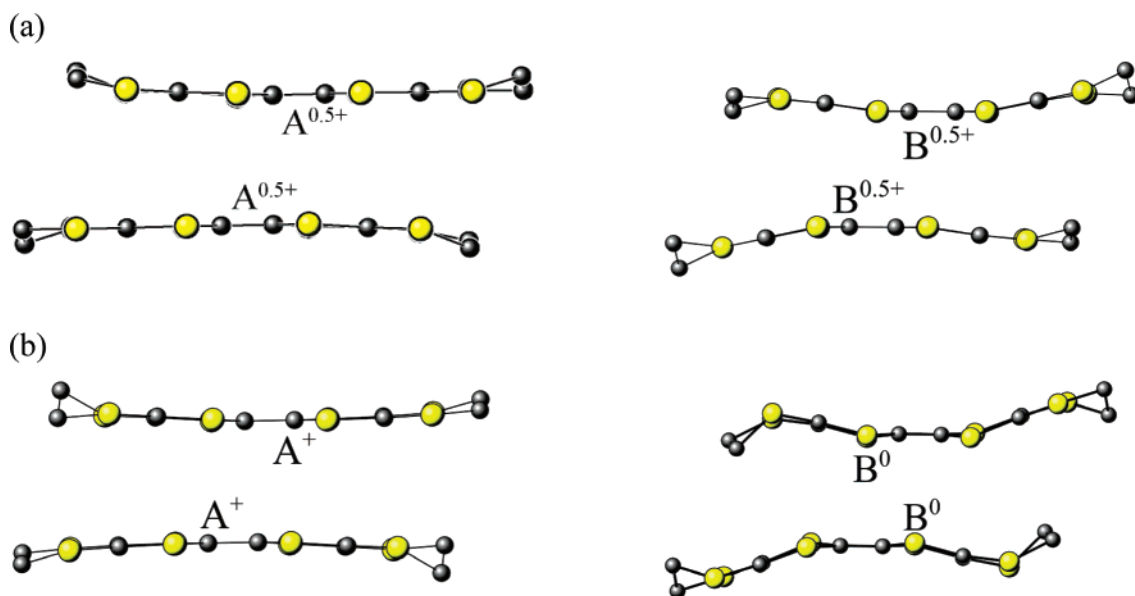


**Figure 2.** Molecular structures of A–A and B–B dimers viewed along the molecular short axis of ET in **1** (a) at RT and (b) at 100 K.

with **2** according to our preliminary measurements. The resistivity of **2** increases by approximately 10% with the evacuation of the air, though the value recovers after the leakage of sample space. This indicates that the evacuation removes the water molecules in the crystal and increases the resistivity. We have found that soaking of the crystal in the oil (Daphne 7373) was sufficient to avoid the influence of evacuation. The electronic band structure was calculated by the tight-binding model based on the extended Hückel method with single- $\xi$  parameters including  $d$ -orbitals for sulfur atoms.<sup>13</sup> The transfer integrals ( $t$ ) were assumed to be proportional to the corresponding overlap integrals ( $S$ ) of the highest occupied molecular orbital (HOMO) of the ET molecules ( $t = -\epsilon S$ ,  $\epsilon = 10$  eV).

### 3. Results and Discussion

**3.1. Crystal Structures.** Crystal structures of **1** and **2** were analyzed at 295 K (RT), 200 K, and around 100 K. In the

present paper, we only describe the structure of **1**, because the two salts are isostructural at each temperature.

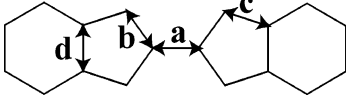
At RT, two crystallographically independent ET molecules, noted **A** and **B**, form two centro-symmetric dimers, A–A and B–B, in the organic layer. The two kinds of the dimers arrange perpendicularly to each other in the  $ab$ -plane, thus creating the  $\kappa$ -type packing pattern (Figure 1). As shown in Figure 2a, the **B** molecule has a slightly warped structure, whereas **A** is almost flat.

Although absolute values of the charges on the ET molecules cannot be estimated from the comparison of the bond lengths according to the usual empirical formula,<sup>14</sup> as a result of the rather poor accuracy of X-ray structural analysis, the central C=C bond lengths are almost the same, 1.370(5) Å for **A** and 1.372(5) Å for **B** (Table 1), indicating

(13) Mori, T.; Kobayashi, A.; Sasaki, Y.; Kobayashi, H.; Saito, G.; Inokuchi, H. *Bull. Chem. Soc. Jpn.* **1984**, *57*, 627.

(14) Guionneau, P.; Kepert, C. J.; Bravic, G.; Chasseau, D.; Truter, M. R.; Kurmoo, M.; Day, P. *Synth. Met.* **1997**, *86*, 1973.



**Table 1.** Selected Bond Lengths (Å) in Molecules **A** and **B** in **1** and **2** at RT and Low Temperatures<sup>a</sup>


		a	b	c	d
<b>1</b> (295 K)	<b>A</b>	1.370	1.734	1.745	1.346
	<b>B</b>	1.372	1.738	1.749	1.352
<b>1</b> (100 K)	<b>A</b>	1.390	1.717	1.737	1.355
	<b>B</b>	1.347	1.757	1.766	1.331
<b>2</b> (295 K)	<b>A</b>	1.373	1.746	1.761	1.345
	<b>B</b>	1.371	1.746	1.759	1.345
<b>2</b> (106 K)	<b>A</b>	1.403	1.719	1.740	1.363
	<b>B</b>	1.350	1.759	1.761	1.342
ET <sup>0</sup> [ref 15a]		1.319	1.757	1.753	1.331
ET <sup>0.5+</sup> [ref 15b]		1.360	1.732	1.744	1.340
ET <sup>+</sup> [ref 15c]		1.388	1.720	1.737	1.345

<sup>a</sup> Average values are used for *b*, *c*, and *d* (see scheme after title). The corresponding values for ET<sup>0</sup>, ET<sup>0.5+</sup>, and ET<sup>+</sup> are given for comparison.

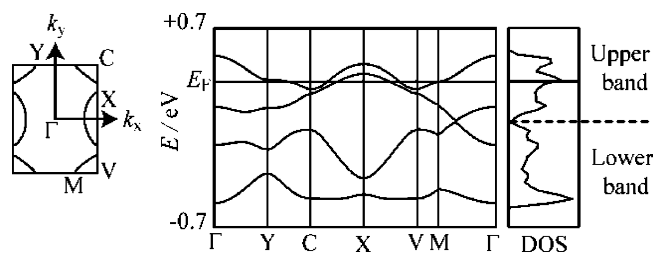
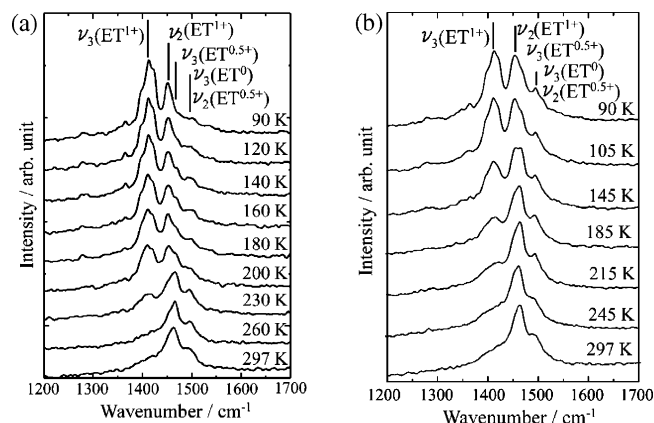
that **A** and **B** have the same mean charge of +0.5 and thus both **A–A** and **B–B** dimers are *S* = 1/2 radicals.

Along the *c*-axis, the ET layer alternates with an inorganic layer, which consists of Co(CN)<sub>6</sub><sup>3-</sup> anions, N(C<sub>2</sub>H<sub>5</sub>)<sub>4</sub><sup>+</sup> cations, and H<sub>2</sub>O molecules. The Co(CN)<sub>6</sub><sup>3-</sup> anion lies on the inversion center, while the N(C<sub>2</sub>H<sub>5</sub>)<sub>4</sub><sup>+</sup> cation is ordered on the twofold axis. The anions are connected to each other along the *b*-axis, through short intermolecular atomic contacts between their terminal N atoms and water molecules (N...O = 2.881(7) Å vs sum of van der Waals radii of 3.07 Å).<sup>16</sup> The successive chains along the *b*-axis form channels in which the N(C<sub>2</sub>H<sub>5</sub>)<sub>4</sub><sup>+</sup> cations are accommodated (see Figure SP5 in Supporting Information).

At 200 K, the crystal system, space group, and molecular shapes of **A** and **B** are essentially the same as those at RT. The central C=C bond length is 1.355(9) Å for **A** and 1.357(9) Å for **B**, indicating that **A** and **B** bear the same charge (+0.5) as at RT.

At 100 K, molecule **B** remarkably deforms as the neutral ET molecule,<sup>17</sup> whereas molecule **A** remains almost flat (Figure 2b) as at RT. The central C=C bond lengths show the distinct difference between the molecules (1.390(9) Å for **A** and 1.347(8) Å for **B**). This is strongly indicative of the charge disproportionation between **A** and **B** such as ET<sup>+</sup> and ET<sup>0</sup>, respectively, which will be discussed below with the Raman spectra. The possible pattern of CO is shown in Figure 1b. Compared to the RT phase, the crystal system and the space group are unchanged, and no superlattice is observed in both **1** and **2**.

**3.2. Electronic Band Structure.** The band structure of **1** at RT, which is based on calculations excluding electron correlation, is given in Figure 3. The HOMO bands substantially split because of the dimerized structure in the

**Figure 3.** Calculated Fermi surface, band dispersion, and density of states (DOS) of **1** at RT.**Figure 4.** Temperature dependence of the FT-NIR Raman spectra of (a) **1** and (b) **2**.  $\nu_3(\text{ET}^n)$  is described in the text.

ET layers, and an average charge of +1/2 per ET leads to a half-filled upper HOMO band. The Fermi surface has a 2D feature with hole-pockets centered at *X* and electron-pockets centered at *C*(*V*), which is closely similar to that of  $\kappa$ -(ET)<sub>4</sub>PtCl<sub>6</sub>·C<sub>6</sub>H<sub>5</sub>CN.<sup>10</sup> It is worth mentioning that this salt behaves as a Mott insulator when the electron correlation is taken into account. Indeed, such calculations give no Fermi surface for the present salts in the CO state. This is clear evidence of the importance of the electron correlation in these systems.

**3.3. Raman Spectra.** Temperature dependence of FT-NIR Raman spectra of salts **1** and **2** within the frequency region of C=C stretching vibrations are displayed in Figure 4. Note that the spectral features of the two salts are almost identical. At 297 K, salt **1** exhibits a distinct band at 1465 cm<sup>-1</sup> accompanied with a shoulder at about 1495 cm<sup>-1</sup>. According to the structural analysis at RT, these bands can readily be ascribed to  $\nu_3(\text{ET}^{0.5+})$  and  $\nu_2(\text{ET}^{0.5+})$ , respectively, even though the latter one seems to overlap with the  $\nu_3(\text{ET}^0)$  band.<sup>18</sup> The observation of a very weak and broad shoulder attributed to  $\nu_3(\text{ET}^+)$  at around 1420 cm<sup>-1</sup> indicates the existence of a small number of ET<sup>+</sup> molecules even at RT.

Whereas the spectral features remain almost invariant down to 260 K, the bands attributed to  $\nu_2(\text{ET}^+)$  at around 1450 cm<sup>-1</sup> and  $\nu_3(\text{ET}^+)$  at around 1410 cm<sup>-1</sup> become pronounced below 230 K. In particular,  $\nu_2(\text{ET}^{0.5+})$  and  $\nu_3(\text{ET}^{0.5+})$  bands remain even at low temperature (200 K). This propensity is seriously inconsistent with the structural

- (15) (a) Kobayashi, H.; Kobayashi, A.; Sasaki, Y.; Saito, G.; Inokuchi, H. *Bull. Chem. Soc. Jpn.* **1986**, *59*, 301. (b) Mallah, T.; Holis, C.; Bott, S.; Kurmoo, M.; Day, P.; Allan, M.; Friend, R. H. *J. Chem. Soc., Dalton Trans.* **1990**, *3*, 859. (c) Triki, S.; Ouahab, L.; Grandjean, D.; Fabre, J.M. *Acta Crystallogr.* **1991**, *C47*, 645.
- (16) Bondi, A. *J. Phys. Chem.* **1964**, *86*, 441.
- (17) Guionneau, P.; Chasseau, D.; Howard, J. A. K.; Day, P. *Acta Crystallogr.* **2000**, *C56*, 453.

- (18) (a) Kozlov, M. E.; Pokhodnia, K. I.; Yurchenko, A. A. *Spectrochim. Acta* **1989**, *45A*, 437. (b) Moldenhauer, J.; Horn, Ch.; Pokhodnia, K. I.; Schweitzer, D.; Heinen, I.; Keller, H. J. *Synth. Met.* **1993**, *60*, 31. (c) Wang, H. H.; Ferraro, J. R.; Williams, J. M.; Geiser, U.; Schluter, J. A. *J. Chem. Soc., Chem. Commun.* **1994**, 1893. (d) Świątek, R.; Lapinski, A.; Ouahab, L.; Yakushi, K. *C. R. Chim.* **2003**, *6*, 395.

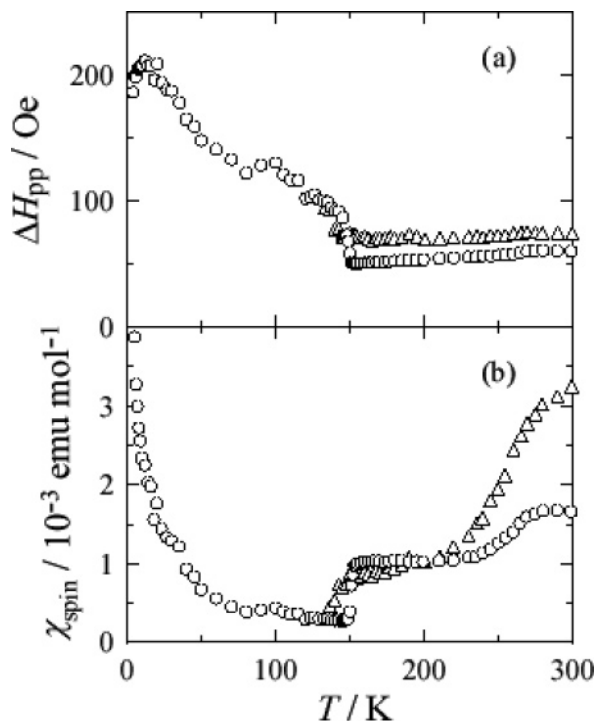


**Figure 5.** Temperature dependence of (a) peak-to-peak line width ( $\Delta H_{pp}$ ) and (b) ESR susceptibility ( $\chi_{spin}$ ) for **1** (circles) and **2** (triangles), applying the static field along the  $a^*$ -axis.

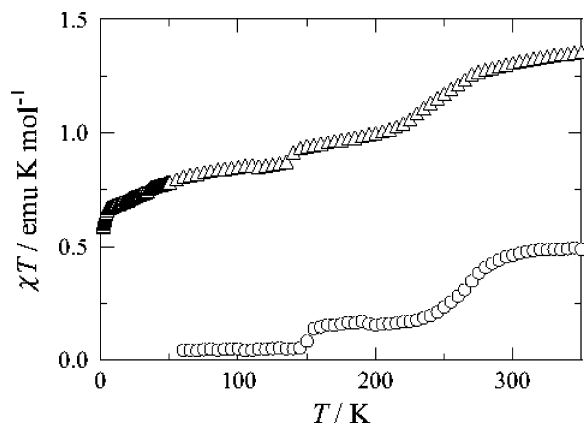


**Figure 6.** Temperature dependence of  $\chi T$  in **1** (circles) and **2** (triangles) in an applied field of 1 T.

analysis at 200 K, which revealed the presence of only  $ET^{0.5+}$  molecules in the crystal. This inconsistency might be explained by the fluctuation of charge order and/or the phase separation, although it should be taken into account that grinding of crystals might influence their properties, for example, yielding some smearing of the CO over a wide temperature range.

Assuming the phase separation of CO and RT phases occurs at around 200 K, the slight difference in the unit cell between the two phases would bring about a change in the profile in each Bragg spot, for example, a splitting. However, no such splitting was observed at 200 K in the X-ray diffraction measurements. Thus it is plausible that the fluctuation of charge order already occurs even at RT and grows extensively below 260 K, resulting in the coexistence of  $ET^+$ ,  $ET^{0.5+}$ , and  $ET^0$ . The gradual decrease of the band  $\nu_3(ET^{0.5+})$  below 150 K indicates that a subtle  $ET^{0.5+}$  remains in the CO phase. A notable point is that the redistribution of

the charge does not occur abruptly, but it is gradually pronounced below 260 K, showing that the fluctuation of charge order develops gradually upon cooling. At 90 K, almost no appearance of the band attributed to  $\nu_3(ET^{0.5+})$  at around  $1470\text{ cm}^{-1}$  allows us to assign the band at around  $1500\text{ cm}^{-1}$  exclusively to  $\nu_3(ET^0)$  instead of  $\nu_2(ET^{0.5+})$ . The Raman spectrum made of the intense  $\nu_2(ET^+)$ ,  $\nu_3(ET^+)$ , and  $\nu_3(ET^0)$  derived from  $ET^+$  and  $ET^0$  is in agreement with the crystal structure analysis of the CO phase at 100 K.

**3.4. ESR Measurements.** At RT a single ESR signal with a Lorentzian shape was observed for **1** at  $g \sim 2$  along all measured directions. The principal values are determined as  $g_1 = 2.0090$ ,  $g_2 = 2.0045$ , and  $g_3 = 2.0036$ , and the axes are in agreement with the crystallographic axes  $c$ ,  $b^*$ , and  $a^*$ , respectively, within the experimental error. The ESR susceptibility ( $\chi_{spin}$ ) at 300 K is  $1.7 \times 10^{-3}$  emu mol $^{-1}$  of formula unit ( $8.5 \times 10^{-4}$  emu mol $^{-1}$  of  $(ET)_2$  dimer). In the temperature range of 280 to 220 K,  $\chi_{spin}$  along the  $a^*$ -axis decreases upon cooling and reaches  $1.0 \times 10^{-3}$  emu mol $^{-1}$  per formula unit at 200 K (Figure 5).

The gradual decrease of  $\chi_{spin}$  down to 200 K would arise either from antiferromagnetic interactions between the fluctuating electrons in the  $(ET^{0.5+})_2$  dimers or from gradual spin annihilation by charge disproportionation from  $(ET^{0.5+})_2 + (ET^{0.5+})_2$  to  $(ET^+)_2 + (ET^0)_2$ , where the latter two species are originally spin-singlet. Peak-to-peak line width of the signal ( $\Delta H_{pp}$ ) remains almost constant down to 150 K, indicating a localized spin system.

The  $\chi_{spin}$  value decreases abruptly at around 150 K as a consequence of the formation of long-range CO, in which both dicationic **A–A** and neutral **B–B** dimers should be spin-singlet. The abrupt change of the signal is in contrast with the gradual spectral change in the Raman spectra. This inconsistency cannot be explained at present but may be related to the different time scale or frequency in ESR and Raman measurements. The ESR intensity below 150 K follows the Curie–Weiss law with 5% of  $S = 1/2$  spins, which cannot be attributed to the conventional defects in CT solids (<1%). Alternately,  $(ET^{0.5+})_2$  dimers with the  $S = 1/2$  spins left behind by CO might contribute to the ESR signal at low temperatures. It is safely concluded that over 95% of the ET molecules in the crystal is in the CO phase below 150 K.

Salt **2** behaves slightly differently from **1** (Figure 5). The  $\chi_{spin}$  value of  $3.2 \times 10^{-3}$  emu mol $^{-1}$  per formula unit at 300 K substantially exceeds that of **1** and even that expected from an uncorrelated two  $S = 1/2$  spins system ( $2.5 \times 10^{-3}$  emu mol $^{-1}$  of formula unit). We think that the exceptionally large  $\chi_{spin}$  is associated with the  $\pi$ - $d$  couplings between ET radical cations and  $Fe(CN)_6^{3-}$  anions through short intermolecular contacts ( $H \cdots N = 2.450(6)\text{ \AA}$  for **B** at RT in **2**). Between 300 and 200 K, the ESR intensity of **2** continuously decreases, corresponding to the successive development of the fluctuation of charge order upon cooling as in the case of **1**. A loss of intensity through the transition at 150 K was also observed in a similar manner to **1**, although the change was more gradual. The line width is almost temperature-independent down to 150 K, where it then begins to increase sharply as in salt **1**. Below 30 K, a distinct signal ac-

accompanied with a hyperfine structure appears, and its intensity increases with decreasing temperature (Curie-like behavior). This signal is unambiguously assigned to the Fe<sup>III</sup> spins of Fe(CN)<sub>6</sub> anions, because it seems that the angular dependence resembles that of Fe<sup>III</sup> spins in K<sub>3</sub>[Fe<sup>III</sup>(CN)<sub>6</sub>].<sup>19</sup>

**3.5. Static Susceptibility Measurements.** The static susceptibility ( $\chi$ ) of the microcrystalline salt **1** is  $1.5 \times 10^{-3}$  emu mol<sup>-1</sup> per formula unit at 300 K, which is very similar to that estimated from the ESR signal. Upon cooling,  $\chi T$  gradually decreases down to around 200 K (Figure 6), corresponding to the development of the fluctuation of charge order. An abrupt drop at 150 K can rationalize the formation of long-range CO. Below 150 K,  $\chi T$  is almost constant and the concentration of spins is estimated to be 5% of  $S = 1/2$  spins.

The  $\chi$  of **2** at 300 K ( $4.0 \times 10^{-3}$  emu mol<sup>-1</sup> of formula unit) is in fairly good agreement with a sum of **1** ( $1.5 \times 10^{-3}$  emu mol<sup>-1</sup> per formula unit) and K<sub>3</sub>[Fe<sup>III</sup>(CN)<sub>6</sub>] ( $2.3 \times 10^{-3}$  emu mol<sup>-1</sup> per formula unit). For  $\chi T$ , a gradual decrease at around 250 K and abrupt drop at 150 K correspond to the development of the fluctuation of charge order and a phase transition to a CO phase, respectively, as in the case of **1** (Figure 6). Below 150 K,  $d$ -spins of Fe<sup>III</sup> ( $S = 5/2$ ) mainly contribute to the susceptibility.

It should be noted that the ESR and static magnetic susceptibility, which are good probes for the electron correlation, of **1** and **2** lie in the range of  $7.5$ – $8.5 \times 10^{-4}$  emu mol<sup>-1</sup> per ET dimer at RT, and the values are intermediate between those of typical Mott insulators such as  $\beta'$ -(ET)<sub>2</sub>X ( $X = \text{ICl}_2$  and  $\text{AuCl}_2$ ;  $9.3$ – $10 \times 10^{-4}$  emu mol<sup>-1</sup>)<sup>20</sup> and the metallic compound  $\beta$ -(ET)<sub>2</sub>AuI<sub>2</sub> ( $3.4 \times 10^{-4}$  emu mol<sup>-1</sup>).<sup>21</sup>

**3.6. Conductivity Measurements.** Figure 7a shows the temperature dependence of resistivity ( $\rho$ ) for **2**. RT conductivity is about 1 S cm<sup>-1</sup>, and  $\rho$  is almost invariable in the temperature range of RT to 280 K. The relatively poor conductivity and large paramagnetic susceptibility, in spite of the calculated Fermi surface, allows us to assert that the salt is on the insulator side of the Mott-Hubbard criterion as in  $\kappa$ -(ET)<sub>2</sub>Cu<sub>2</sub>(CN)<sub>3</sub> and  $\kappa$ -(ET)<sub>2</sub>Cu[N(CN)<sub>2</sub>]Cl.<sup>1,6</sup> It was found that both  $\kappa$ -(ET)<sub>2</sub>Cu<sub>2</sub>(CN)<sub>3</sub> and  $\kappa$ -(ET)<sub>2</sub>Cu[N(CN)<sub>2</sub>]Cl exhibited similar conductivity ( $2$ – $7$  S cm<sup>-1</sup> at RT) with higher activation energy for conduction ( $\epsilon_a = 0.012$ – $0.05$  eV)<sup>9a,22</sup> and smaller  $\chi_{\text{spin}}$  values ( $4.5$ – $5.5 \times 10^{-4}$  emu mol<sup>-1</sup> per ET dimer at RT).<sup>4,23</sup> Although the large  $\chi_{\text{spin}}$  values for **1** and **2** suggest that the electron correlation is much stronger, the negligible  $\epsilon_a$  values indicate that the electrons in **1** and **2** are more itinerant in nature than those of  $\kappa$ -(ET)<sub>2</sub>X ( $X = \text{Cu}_2(\text{CN})_3$ ,  $\text{Cu}[\text{N}(\text{CN})_2]\text{Cl}$ ). The nearly temperature indepen-

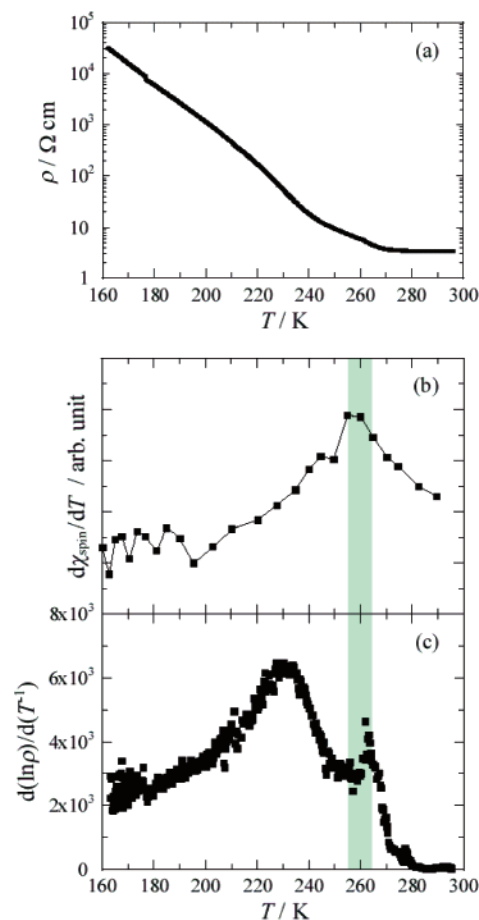


**Figure 7.** Temperature dependence of (a) resistivity ( $\rho$ ), (b)  $d\chi_{\text{spin}}/dT$ , and (c)  $d(\ln \rho)/d(T^{-1})$  for **2**.

dent behavior of resistivity above 280 K may be explained by the presence of the fluctuation of charge order (mixing of  $\text{ET}^{0.5+}$ ,  $\text{ET}^+$ , and  $\text{ET}^0$ ) which exists even at RT as confirmed by Raman spectrum (Figure 4), because the interdimer Coulomb repulsion prevents each carrier from being localized on a dimer. The temperature dependence of  $d(\ln \rho)/d(T^{-1})$  shows an increase below 280 K upon cooling (Figure 7c), indicating the development of the fluctuation of charge order as shown in the Raman spectra. The magnetic susceptibility also decreases below about 280 K. The peak in  $d(\ln \rho)/d(T^{-1})$  at 265 K corresponds to the inflection point of the magnetic susceptibility as shown in Figure 7b, indicating the rapid development of the fluctuation of the charge order.

**3.7. Mechanism of the Phase Transition.** In the  $\kappa$ -phase salts with strong dimerization of donor molecules, the intradimer on-site Coulomb repulsion  $U_{\text{eff}}$  plays an essential role to stabilize the Mott insulating state, where the  $(\text{ET}^{0.5+})_2$  dimer forms a uniform 2D array (Figure 1). On the other hand, the Coulomb interaction between the neighboring dimers ( $V_d$ ) favors the CO between dimers. It was argued theoretically that the  $\kappa$ -phase may show various ground states; AF, CO, and paramagnetic states, depending on the long-range Coulomb interaction.<sup>24</sup> At RT, a  $(\text{ET}^{0.5+})_2$  dimer is surrounded by the six nearest neighboring  $(\text{ET}^{0.5+})_2$  dimers.

(19) Baker, J. M.; Bleaney, B.; Bowers, K. D. *Proc. Phys. Soc.* **1956**, *B69*, 1205.

(20) Yoneyama, N.; Miyazaki, A.; Enoki, T.; Saito, G. *Bull. Chem. Soc. Jpn.* **1999**, *72*, 639.

(21) Talham, D. R.; Kurmoo, M.; Day, P.; Obertelli, D. S.; Parker, I. D.; Friend, R. H. *J. Phys.* **1986**, *C19*, 383.

(22) Williams, J. M.; Kini, A. M.; Wang, H. H.; Carlson, K. D.; Geiser, U.; Montgomery, L. K.; Pyrka, G. J.; Watkins, D. M.; Kommers, J. M.; Boryschuk, S. J.; Crouch, A. V.; Kwok, W. K.; Schirber, J. E.; Overmyer, D. L.; Jung, D.; Whangbo, M. H. *Inorg. Chem.* **1990**, *29*, 3272.

(23) Miyagawa, K.; Kawamoto, K.; Nakazawa, Y.; Kanoda, K. *Phys. Rev. Lett.* **1995**, *75*, 1174.

(24) Imamura, Y.; Ten-no, S.; Yonemitsu, K.; Tanimura, Y. *J. Chem. Phys.* **1999**, *111*, 5986.



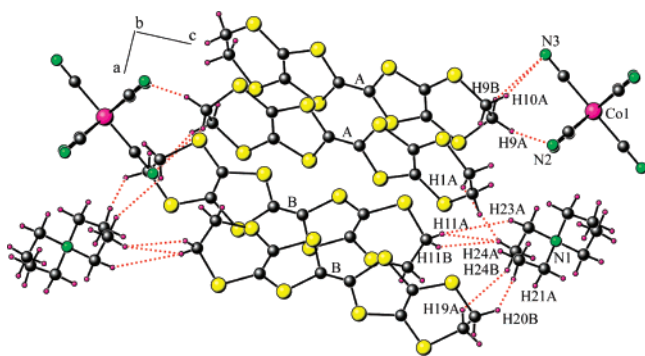


**Figure 8.** Intermolecular contacts between anions, cations, and **A** and **B** molecules. Dashed lines indicate N...H and H...H intermolecular contacts shorter than 3.0 Å.

**Table 2.** Shortest Intermolecular Distances (Å) between Anions or Cations and **A** and **B** Molecules at RT and Low Temperatures

		1 (RT)	2 (RT)	1 (100 K)	2 (106 K)
anion... <b>A</b>	N3...H10	2.582	2.579	3.032	3.053
	N3...H9	3.175	3.294	2.844	2.880
	N2...H9	2.704	2.751	2.797	2.816
anion... <b>B</b>	N3...H12	2.387	2.389	2.597	2.573
	N4...H19	2.666	2.676	2.765	3.447
cation... <b>A</b>	H24...H2	2.541	2.563	2.495	2.650
	H21...H2	2.596	2.610	3.075	2.880
	H24...H1	2.966	3.021	3.117	3.342
cation... <b>B</b>	H11...H24	2.673	2.683	2.821	2.913
	H11...H23	2.929	2.871	2.776	2.492
	H21...H20	2.723	2.700	2.439	2.460
	H24...H19	2.789	2.786	2.691	2.783

Therefore, the Coulomb energy per unit cell is roughly estimated as  $6V_d$ . On the other hand, there are only two nearest neighboring  $(\text{ET}^+)_2$  dimers for a  $(\text{ET}^+)_2$  dimer in the CO phase, and  $(\text{ET}^0)_2$  dimers do not contribute to  $V_d$ . Therefore, the Coulomb energy per unit cell is evaluated as  $U_{\text{eff}} + 4V_d$  in the CO state. The competing effect of  $U_{\text{eff}}$  and  $V_d$  would be essential for the fluctuation of charge order and the phase transition.

We should also consider the role of electrostatic interactions such as donor...anion and donor...cation interactions in the phase transition. Because **A** and **B** are crystallographically independent, it is apparent that the distances to the inorganic components are not the same for **A** and **B**, resulting in different Coulomb potentials.<sup>10b</sup> The shortest intermolecular distances of **A** and **B** with  $\text{M}(\text{CN})_6^{3-}$  and  $(\text{C}_2\text{H}_5)_4\text{N}^+$  are given in Table 2 and Figure 8. One can notice in particular that (i) the distances between the  $\text{M}(\text{CN})_6^{3-}$  anion and **B** increase when  $T$  decreases, (ii) the distances between  $(\text{C}_2\text{H}_5)_4\text{N}^+$  and **A** increase when  $T$  decreases, and (iii) the distances between  $(\text{C}_2\text{H}_5)_4\text{N}^+$  and **B** decrease when  $T$  decreases. These three structural changes show clearly that the Coulomb potentials are modified through the phase transition and contribute to the stabilization of the CO phase. Actually, the stripe pattern of CO, which is parallel to the  $b$ -axis, coincides with the arrangement of anion layers, where the chains of  $\text{M}(\text{CN})_6^{3-}$  and  $(\text{C}_2\text{H}_5)_4\text{N}^+$  are parallel to the  $b$ -axis.

The strong electron–electron correlation of  $\pi$ -electrons and Coulomb interaction between ET and inorganic layers plays a key role in the present salts. Moreover, the spin entropy plays a role in the transition, because the spin degrees

of freedom vanish in the CO phase with spin-singlet ground state. It is also considered that the flexibility of the donor molecule and the presence of discrete anions with highly negative charge are responsible for the large charge difference between **A** ( $\text{ET}^+$ ) and **B** ( $\text{ET}^0$ ) in the CO phase. The significant deformation of neutral **B** exerts an effect in some way that leads to the HOMO level of **B** lower than that of **A** by 0.25 eV, giving rise to the charge disproportionation between **A** and **B**.

The most interesting feature in the present salts is the gradual development of the fluctuation of charge order. Such a behavior indicates the competition of the two phases. It is plausible that the intra-dimer Coulomb interaction is comparable to the inter-dimer Coulomb interaction in these salts.

## Conclusion

The two new CT salts  $\kappa\text{-(ET)}_4[\text{M}(\text{CN})_6][\text{N}(\text{C}_2\text{H}_5)_4]\cdot 2\text{H}_2\text{O}$  ( $\text{M} = \text{Co}^{\text{III}}$  and  $\text{Fe}^{\text{III}}$ ) were synthesized, and their crystal structures and physical properties were investigated. The salts are isostructural to each other and contain two kinds of dimerized molecules in the conducting  $ab$ -plane. At RT, the two crystallographically independent ET molecules possess an equivalent charge of +0.5 and behave as Mott insulators. The temperature dependence of Raman spectra revealed that the CO occurs very gradually. The crystallographic studies performed at different temperatures provide us with further confirmation of the charge disproportionation at low temperatures. The magnetic susceptibility decreased gradually with decreasing temperature in accordance with the gradual CO. In addition, we observed the abrupt change in the ESR susceptibility and the line width at 150 K, indicating a transition from a Mott insulating phase with the fluctuation of charge order to a long-range CO state. Coulomb interaction plays the essential role in determining the physical properties including conducting, optical, and magnetic properties. The electrostatic Coulomb potentials of the counter components in the inorganic layer are necessary to give the different environments for the crystallographically independent ET molecules. This effect and the flexibility of the ET molecule are directly related to the pattern of CO, which is composed of a bent  $\text{ET}^0$  dimer and a flat  $\text{ET}^+$  dimer. The competition between  $U_{\text{eff}}$  and  $V_d$  is essential for the fluctuation of charges and the peculiar phase transition. The above-discussed features are correlated and cooperative, that is, the molecular degree of freedom is combined with the electronic correlation in the low dimensional system, and thus unusual physical properties and phase transition are generated in these CT salts.

**Acknowledgment.** This work was supported in part by the CNRS-JSPS PICS Project No. 1433, a Grant-in-Aid for JSPS research fellows, JSPS Core-to-Core Program “Multifunctional Molecular Materials and Device Applications”, a COE Research on Elements Science (No. 12CE2005), a Grant-in-Aid (21st Century COE program on Kyoto University Alliance for Chemistry), the Grant-in-Aid for Scientific Research (No. 15205019 by JSPS) and la Région Bretagne with Projects SIE No. 05012917 and PRIR No. 05013053. R.Š. is indebted to the Center of Excellence for Magnetic and Molecular Materials for

Future Electronics within the European Commission Contract No. G5MA-CT-2002-04049. We thank Dr. J.F. Halet (Université de Rennes 1) for reading the manuscript before publication.

**Supporting Information Available:** Crystallographic data in CIF format for the structures reported in this paper and ORTEP, crystal packing views of **1** at RT, Raman spectra of **2**, angular

dependence of the  $g$ -factor of **1** at RT, and ESR spectra of **2** at 4 K, including also a table for the HOMOs of ET molecules (*E*) and *S* (PDF). This material is available free of charge via the Internet at <http://pubs.acs.org>.

CM063036K